Analysis of the vibracoustic behavior of a plate excited by synthetized aeroacoustic pressure fields

Denis Ricot, Abbas Hekmati, Philippe Druault

ACOUSTICS 2012

Analysis of the vibracoustic behavior of a plate excited by synthetized aeroacoustic pressure fields

D. Ricot[a], A. Hekmati[b] and P. Druault[c]

[a]RENAULT, Research Advanced Engineering and Materials Department, TCR AVA 1 63, 1 av. du Golf, 78288 Guyancourt, France
[b]TECHNOCENTRE RENAULT, TCR AVA 1 63, 1 av. du Golf, 78288 Guyancourt, France
[c]Institut Jean Le Rond d'Alembert, Boite 162 4 place Jussieu 75005 Paris
denis.ricot@renault.com

Due to acoustic comfort has become one of the principal concerns for car manufacturers, it is important to improve i) the knowledge of the car panel vibrations which are due to two different components: acoustic excitation and turbulent wall pressure one, and ii) the associated radiation in the car interior. In this paper, first, we propose to synthetize such aeroacoustic wall pressure field based on Cholesky decomposition. Using analytical expressions of the Cross Power Spectral Density of an acoustic diffuse field and of a turbulent flow (Corcos's model), spatial distributions of turbulent and acoustic excitations are determined. Then, as a second step, the vibroacoustic behavior of a plate excited by these synthetized fields is computed thanks to FEM calculations (ACTRAN software). The radiated field is then successively estimated for the acoustic excitation, the turbulent one and for both aeroacoustic excitations. The effect of flow inhomogeneity on the vibroacoustic behavior of the plate has been also regarded. Finally, a statistical analysis between radiated field and excitation fields is performed thanks to the coherence function analysis. It is then confirmed that such analysis presents some limits especially when dealing with uncorrelated sources of noise.

1 Introduction

A way to improve the acoustic comfort of vehicle passengers is to reduce the source of noise radiated in the interior vehicle. More precisely, for high velocities, the car panel vibrates under the influence of the aerodynamic exterior flow and it contributes to a non negligible noise radiation part in the car interior. The car panel vibrations are due to two different components: an acoustic excitation (emitted and generated in the exterior aerodynamic flow) and a turbulent component (development of turbulent boundary layer flow over the car panel). Note that the summation of both excitation components will be denote in the following: aeroacoustic component. These both components have quite different characteristics (energy, wavenumber representation, propagation velocities, *etc*) [1, 2]. To improve the knowledge of the car panel vibrations and the associated radiation in the car interior, we propose to use classical models for representing each wall pressure component. The use of such models allows then the investigation of the vibroacoustic response of a car panel by means of Finite Element Methods.

Generally, these excitation components are well represented thanks to their statistical properties by means of their Cross Power Spectral Density (CPSD) functions. However for particular applications and/or post-processing analyses, it is necessary to represent the wall pressure field in the time-space domain. As a first challenge, we propose in this paper the reconstruction of a random wall pressure distribution from the knowledge of their CPSD. The spatial representations of wall turbulent pressure field as well as of the acoustic pressure field are then obtained for each retained frequency (Part 2 of this paper). The second challenge consists in performing FEM calculations (Part 3) based on these synthetized pressure fields. The vibroacoustic behavior of a rectangular plate is then analyzed as a function of the excitation pressure field (either a purely turbulent excitation or a purely acoustic excitation or an aeroacoustic excitation). In Part 4, it is successively analyzed i) the transmission efficiency of homogeneous pressure field as a function of the type excitation field; ii) the inhomogeinity effect of the turbulent component on transmission efficiency; iii) the correlation which exists between radiated pressure field and excitation fields.

2 Synthesis of wall pressure fields

In this part, it is proposed to determine the random wall pressure fluctuations, $p(x_i, t)$ from the knowledge of its statistical properties that is the Cross Power Spectral Density (CPSD). Before presenting this synthesis method based on Cholesky decomposition, the mathematical expression of the CPSD associated with the turbulent component as well as the acoustic component are recalled.

2.1 CPSD representations of turbulent and acoustic excitation components

To represent the turbulent component, the classical Corcos's Model [5] is considered. Assuming a two dimensional car panel (plane (O, x, y)), the following analytical expression of the CPSD associated with the turbulent wall pressure field is then used:

$$S_{pp}^{Corcos}(\mathbf{x}_i, \mathbf{x}_j, \omega) = S_{pp}^{Corcos}(\omega) e^{-|\omega r_x|/(\alpha_1 U_c)} e^{-|\omega r_y|/(\alpha_2 U_c)} e^{-i\omega r_x/U_c} \tag{1}$$

where α_1 and α_2 indicate the correlation coefficients in x and y directions respectively. These coefficients are directly related to the integral scales in the corresponding directions. U_c represents the convection velocity of the flow.

According to the acoustic component representation, a diffuse acoustic field is considered and it is expressed in the spectral domain as follows:

$$S_{pp}^{Diffuse}(\mathbf{x}_i, \mathbf{x}_j, \omega) = S_{pp}^{Diffuse}(\mathbf{r}, \omega) = S_{pp}^{Diffuse}(\omega) \frac{sin(k_0 r)}{k_0 r} \tag{2}$$

with $\mathbf{r} = x_j - x_i$ and $k_0 = \omega/c_0$, c_0 is the sound propagation velocity. The summation of this acoustic component and this turbulent one of the wall pressure field are then supposed to represent both fields that contribute to the car panel excitations.

2.2 Cholesky decomposition of CPSD matrix

Assuming the CPSDs of the excitation fields are known, the first challenge consists in explaining a realization n, $p^{(n)}(\mathbf{x}_i, \omega)$ of the wall pressure fields associated with each excitation (acoustic and turbulent component). Then using an inverse FFT in the temporal-frequency domain, the determination of a particular wall pressure realization, $p^{(n)}(\mathbf{x}_i, t)$, is then conceivable [9]. In the following, the first step implementation is presented.

Wittig *et al.* [10] proposed a procedure in order to simulate multicorrelated random processes and more recently Coyette [6] proposed to use this procedure in the framework of wall pressure fluctuations. Wittig *et al.* [10] assumed that the one sided CPSD matrix can be factored

into a lower triangular matrix and its complex transpose (Cholesky decomposition):

$$G_{pp}(\mathbf{x}_i, \mathbf{x}_j, \omega) = H_{pp}(\mathbf{x}_i, \mathbf{x}_j, \omega) H^*_{pp}(\mathbf{x}_j, \mathbf{x}_i, \omega)\ . \quad (3)$$

where the one sided CPSD function is defined as follows: $G_{pp}(\mathbf{x}_i, \mathbf{x}_j, \omega) = 2S_{pp}(\mathbf{x}_i, \mathbf{x}_j, \omega)$ if $\omega > 0$, and $G_{pp}(\mathbf{x}_i, \mathbf{x}_j, \omega = 0) = S_{pp}(\mathbf{x}_i, \mathbf{x}_j, \omega = 0)$. Then, one realization (n) of pressure field can be obtained:

$$p^{(n)}(\mathbf{x}_i, \omega) = \sum_{j=1}^{M} H_{pp}(\mathbf{x}_i, \mathbf{x}_j, \omega)\Gamma_j^{(n)} \text{ with } \Gamma_j^{(n)} = e^{i\phi_j} \quad (4)$$

where ϕ_j is an arbitrary random phase: $\phi_j = rand\,[0, 1] \times 2\pi$ with $j = 1, \cdots, M$. with M the total number of grid points meshing the plate. We then perform $N = 30$ realizations independently for each component on the surface of a plate:

$$p^{Corcos(n)}(\mathbf{x}_i, \omega) = \sum_{j=1}^{M} H_{pp}^{Corcos}(\mathbf{x}_i, \mathbf{x}_j, \omega)\Gamma_j^{(n)} \quad n = 1, 30 \quad (5)$$

$$p^{Diffuse(n)}(\mathbf{x}_i, \omega) = \sum_{j=1}^{M} H_{pp}^{Diffuse}(\mathbf{x}_i, \mathbf{x}_j, \omega)\Gamma_j^{(n)} \quad n = 1, 30 \quad (6)$$

Based on these spatial representations of each excitation component, the CPSD is computed in order to compare to the available analytical expressions of the CPSD. Such analysis allows an investigation of the effect of the synthesis procedure on the CPSD representation and especially the effect of the number N of realizations. Figure 1 shows the sum of Corcos and diffuse CPSD functions. Figure 1 (a) shows the CPSD as a function of frequency for a given separation distance ($\mathbf{x}_1(0, 0, 0)$ and $\mathbf{x}_2(0.08, 0, 0)$). Figure 1 (b) shows the CPSD calculated between the central point ($\mathbf{x}_1(0, 0, 0)$) and all the points situated on the line $(x_1, 0, 0)$ for a given frequency. When using a high number of realizations (for instance 1000), the estimation of CPSD via these pressure field realizations approaches the analytical CPSD.

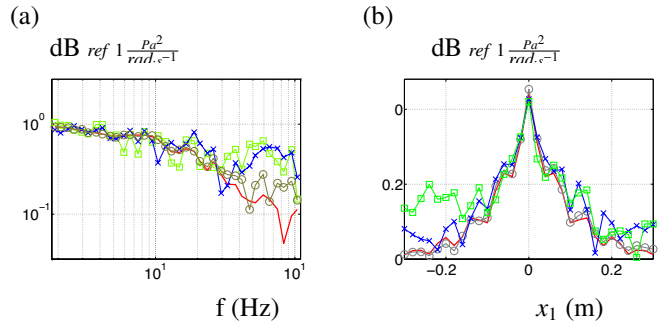

Figure 1: The analytical expression (—) and the estimation by (⊡) 20, (×) 30 and (○) 1000 realizations of Corcos plus diffuse CPSD functions. (a) As a function of the frequency for a given separation distance of 0.08 m ($\mathbf{x}_1(0, 0, 0)$ and $\mathbf{x}_2(0.08, 0, 0)$). (b) As a function of the separation distance on the $(x_1, 0, 0)$ line at a given frequency of $f = 520$ Hz.

3 FEM calculation

Figure 2 displays the computational set-up of the vibratory and radiation calculations performed thanks

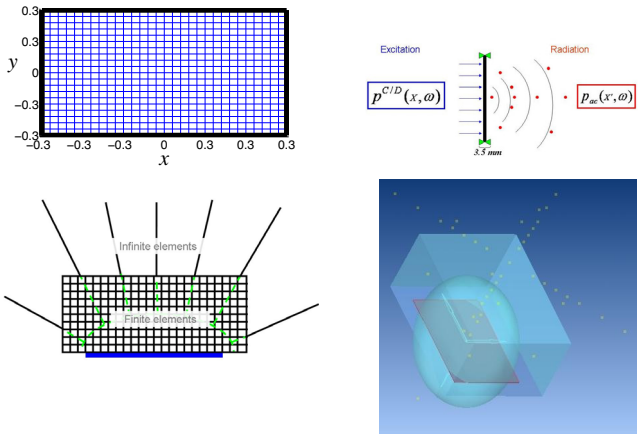

Figure 2: Computational set-up. The radiated acoustic pressure field is calculated for a simply supported plate by mean of finite and infinite elements. The infinite elements start from the last finite elements and are normal to the support ellipsoid. 50 probes are considered in order to estimate the radiated acoustic pressure field.

to ACTRAN[11]. A rectangular plate of dimension $L_x = 0.6$ m, $L_y = 0.4$ m and $L_z = 0.0035$ m is meshed using shell elements of size $\Delta_x = \Delta_y = 0.02$ m and $\Delta_z = 0.004$ m. The mechanical characteristics of the glass $E = 4.85E10 + i2.425E9$ Pa, $\upsilon = 0.2398$, $\rho = 2500$ kg/m^3 and the simply supported boundary conditions are considered. The characteristic acoustic coincidence frequency can be calculated using the equation:

$$f_0^c = \frac{c_0^2}{2\pi}\sqrt{\frac{12\rho(1-\upsilon^2)}{Eh^2}}. \quad (7)$$

For this plate, the acoustic coincidence frequency is $f_0^c = 4136$ Hz. For turbulent boundary layer excitation, the aerodynamic coincidence frequency is calculated using equation (7) by replacing the sound speed with convection velocity of $U_c = 36$m/s. We obtain $f_c^c = 45$ Hz.

Thirty six frequencies logarithmically distributed between 185 and 10000 Hz are considered. The radiated acoustic pressure field is calculated by an ensemble of the finite and infinite elements. In this region a mesh size of 0.02 m is considered for : $-0.4 \leq x' \leq 0.4$, $-0.3 \leq y' \leq 0.3$ and $0 \leq z' \leq 0.4$ providing a total number of 24600 finite elements. As shown in figure 2 for the rest of space the infinite acoustic elements are considered. The radiated acoustic pressure is also probed at 50 individual points to future investigate the relationship between excitation and radiated fields. Note that the mesh interval $\Delta_x = 0.02$ m associated with the mean flow velocity $U_c = 36$ m/s, for turbulent excitation and consequently aeroacoustic excitation can not permit to investigate frequencies higher than 900 Hz due to the non-respect of the Nyquist-Shannon criterion.

4 Results

In the following, the transmission efficiency of a given excitation field is evaluated by:

$$\tau(\omega) = \frac{\Pi_{ac}(\omega)}{(L_x \times L_y) S_{pp}(\omega)} = \frac{\frac{1}{N}\sum_n \Pi_{ac}^{(n)}(\omega)}{(L_x \times L_y)\frac{1}{N}\sum_n S_{pp}^{(n)}(\omega)}. \quad (8)$$

$\Pi_{ac}^{(n)}(\omega)$ indicates the radiated acoustic power given by :

$$\Pi_{ac}^{(n)}(\omega) = \lim_{T\to+\infty} \frac{2\pi}{T} \int_{\Omega'} Re\left\{p_{ac}^{(n)}(\mathbf{x}',\omega,T)v^{*(n)}(\mathbf{x}',\omega,T)\right\} d\mathbf{x}', \tag{9}$$

where * indicates the complex conjugate, $v^{(n)}(\mathbf{x}',\omega,T)$ represents the vibration velocity field and Ω' indicates the radiating surface of the plate. For the sake of the simplicity, the space variable in the radiation side of the plate for the point i is indicated by $\mathbf{x}_i'$. Recall that the same energy level is considered for all realization of a given type of excitation, $S_{pp}(\omega) = S_{pp}^{(n)}(\omega)$.

To perform radiation analyses as a function of excitation components, the following coherence function γ is used:

$$\gamma^2(\mathbf{x}_i,\mathbf{x}_j',\omega) = \frac{\left|\sum_{n=1}^{N} p^{(n)}(\mathbf{x}_i,\omega)p^{(n)*}(\mathbf{x}_j',\omega)\right|}{(\sum_{n=1}^{N} p^{(n)}(\mathbf{x}_i,\omega)p^{(n)*}(\mathbf{x}_i,\omega))(\sum_{n=1}^{N} p^{(n)}(\mathbf{x}_j',\omega)p^{(n)*}(\mathbf{x}_j',\omega))}$$

This coherence function allows the calculation of the correlation in the frequency domain between two signals located on the plate (x_i location) and in the radiated field (x_j' location). for a spatially averaged correlation, the following mean coherence value is computed:

$$\overline{\gamma}^2(\omega) = \frac{1}{M_{\mathbf{X}} M_{\mathbf{X}'}} \sum_{i=1}^{M_{\mathbf{X}}} \sum_{j=1}^{M_{\mathbf{X}'}} \gamma^2(\mathbf{x}_i,\mathbf{x}_j',\omega) \tag{10}$$

with $M_{\mathbf{X}}$ and $M_{\mathbf{X}'}$ the total numbers of available grid points on the flat plate domain and in the radiated domain.

4.1 Transmission efficiency of homogeneous pressure fields

The first analysis deals with the investigation of the transmission efficiency of an aeroacoustic excitation and its acoustic and turbulent components. Based on FEM calculations, the vibroacoustic responses of the simply supported rectangular plate excited by each realization of the synthetic fields $p^{Corcos(n)}(\mathbf{x}_i,\omega)$, $p^{Diffuse(n)}(\mathbf{x}_i,\omega)$ and both $p^{Corcos(n)}(\mathbf{x}_i,\omega) + p^{Diffuse(n)}(\mathbf{x}_i,\omega)$ are independently studied. To approach realistic energetic configuration, we considered $S_{pp}^{Diffuse}(\omega) = 0.1 \times S_{pp}^{Corcos}(\omega) = 6.4$ Pa$^2/rad.s^{-1}$ that corresponds to 92 dB (acoustic diffuse field) and 102 dB (turbulent component). The same energy is imposed for each frequency. Figure 3 (left hand side) shows PSD of the fluctuating pressure spectrum for each excitation field for a selected point of the plate at $(x,y,z) = (0.1, 0.16, 0)$.

Figure 3 (right hand side) shows the PSD of the radiated acoustic pressure related to different excitation fields in $(x',y',z') = (0,0,0.6)$. For a constant excitation spectrum, the radiated spectrum should decrease regularly due to the increase of global isolation efficiency of standard plates as the frequency rises. This decreasing radiated spectrum is well observed for the acoustic excitation case in figure 3 (right hand side-top). In figure 3 (right-hand side-center) and (right-hand side-bottom), the increase of the radiated pressure spectrum from 900 Hz for turbulent pressure field and from 3000 – 4000 Hz for aeroacoustic pressure field is due to the spatial aliasing effects of the excitation field. This aliasing effect is also visible for the radiated field related to the aeroacoustic excitation (figure 3 (right hand side-bottom) but it seems to occur at higher frequency comparing to

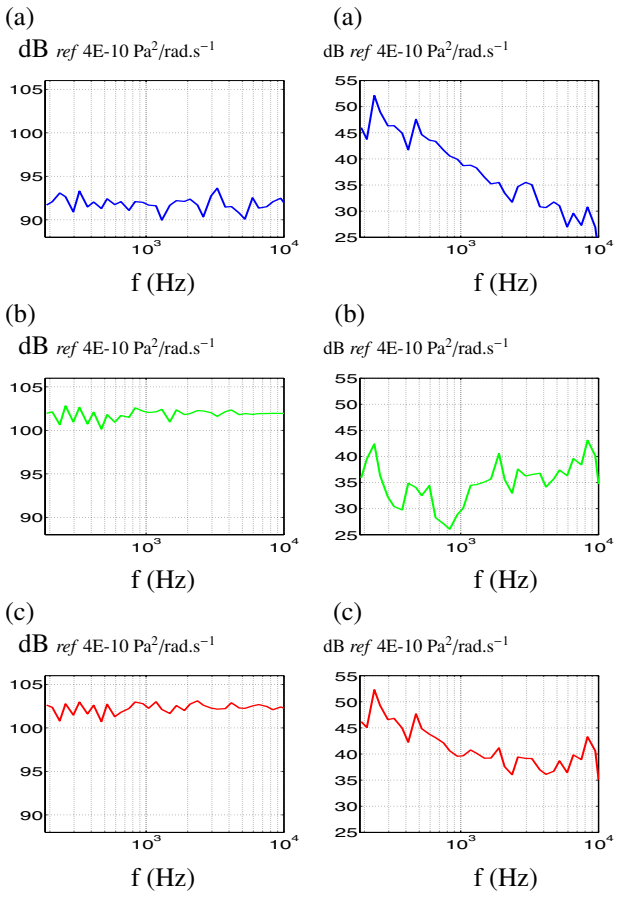

Figure 3: Left hand side: PSD of excitation pressure fluctuation in a given point of plate: (top to bottom) a) acoustic (b) turbulent (c) aeroacoustic. Right hand side: PSD of radiated pressure fluctuation at 0.6m from the plate, $(x',y',z') = (0,0,0.6)$: (top to bottom) (a) acoustic pressure excitation, (b) turbulent pressure excitation and (c) aeroacoustic excitation.

the one associated to the purely turbulent excitation. This is mainly related to the acoustic part in the aeroacoustic excitation as the radiated pressure level is mostly influenced by this acoustic excitation.

In figure 3 (right-hand side), one can notice that the radiated acoustic field associated with the diffuse field excitation is almost 10 dB superior to the one related to the turbulent excitation field. Figures 3 reveals that the acoustic excitation is much more efficient than the turbulent excitation in producing the acoustic radiation. In fact, while the acoustic excitation is 10 times less energetic than the turbulent one, the radiated field related to the acoustic excitation is 10 times more energetic than the one related to the turbulent excitation. This means that the acoustic excitation is 100 times more efficient than the turbulent excitation for most of the validated studied frequencies.

In fact, the acoustic pressure probed at particular direction and position cannot accurately represent the complete radiated field. Then, the transmission efficiency analysis based on the radiated acoustic pressure in a single point could be improper. For a more precise study the transmission efficiency is evaluated by the equation (8). Figure 4(b) shows the value of $\tau(\omega)$ for each excitation type as a function of frequency. In agreement with previous analysis the transmission efficiency of acoustic excitation

clearly appears to be 100 times higher than the transmission efficiency of the turbulent excitation. We can also observe that the coincidence frequency mechanism for the acoustic excitation appears at around 3900 Hz, value which is suitably close to the analytical one 4136 Hz, given by the equation (7).

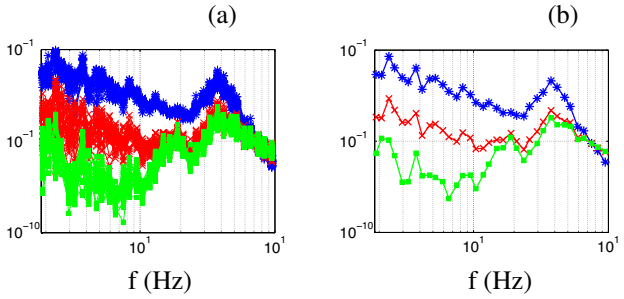

Figure 4: Transmission efficiency of (∗) acoustic excitation, (▪) turbulent excitation (×) aeroacoustic excitation. (a) All pressure field realizations, (b) averaged on realizations

Figure 4(a) shows the transmission efficiency related to each realization : $\Pi_{ac}^{(n)}(\omega)/(L_x \times L_y)S_{pp}(\omega)$. Although the mean pressure field is constant for each realization of a particular excitation category, the obtained results are different for each realization. This dispersion is related to the random phases considered in the field generation procedure.

In the frequency range 200-900 Hz which avoids any aliasing errors, figure 4(b) clearly shows that the transmission efficiency of the acoustic field is 100 times (i.e. 20 dB) higher than that of the turbulent field for the chosen Corcos and plate parameter sets. This result is in agreement with the study of Bremner and Wilby [4] based on Statistical Energy Analysis. They explained that the acoustic power radiated by a glass panel submitted to an acoustic field at a given level is 15 to 30 dB higher than the acoustic power radiated by the same panel excited by a turbulent field with the same level. The higher efficiency of the acoustic excitation field is mainly related to its larger wavelengths that can be more easily coupled with the radiating modes of the plate that include mainly large wavelengths. Below the acoustic coincidence frequency, the radiating modes are the non-resonant structural modes that are driven by mass.

4.2 Transmission efficiency of inhomogeneous pressure fields

From a realistic point of view, turbulent wall pressure field over a car panel is fully inhomogeneous [7]. In this sense, the wall pressure synthesis has to take into account such property to approach the realistic flow configuration. In a previous papers, Hekmati *et al.* [8, 9] described a method to reproduce such inhomogeneous flow configuration. They also analyzed the vibroacoustic answer of a plate excited by such an inhomogeneous turbulent flow field. Here, we only recall these previous results.

To synthetize an inhomogeneous wall pressure flow field, the surface plate is divided in two regions where two homogeneous fields are imposed and both mean flow directions make an angle of 60^o. The Corcos's model is then considered to reproduce the CPSD of boundary layer flow in each homogeneous region. An hyperbolic function is used between both homogeneous regions in order to have a smoother transition between both regions. It was first demonstrated that deterministic inhomogeneous wall pressure fields can be similarly obtained thanks to the Cholesky decomposition described above. These deterministic signals were then used as inhomogeneous field to examine the inhomogeneity effect on the plate transmission. By comparing results computed from homogeneous 'equivalent' excitation fields and those deduced from inhomogeneous turbulent excitation, we shown that the inhomogeneity of the excitation field has little influence on the global behavior of the plate. Indeed, quasi-similar results were obtained when dealing with 'equivalent' homogeneous excitation fields.

4.3 Coherence function analysis between the radiated and excitation fields

Based on numerical results, a coherence function analysis is performed to investigate the link that exists between radiated pressure field and homogeneous excitation fields. Several FEM calculations are carried out using as excitation fields: a purely acoustic excitation, a purely turbulent excitation and an aeroacoustic excitation. To reproduce a representative energy repartition, the turbulent component is supposed to be 10dB superior to the one associated with the acoustic component. Figure 5 displays the resulted mean coherence representation as a function of the frequency. Note that figure 5 (bottom) represents the mean coherence evolution computed between the radiated field and either the acoustic component or the turbulent component or both components, for one FEM calculation.

It is first observed that a very low level of mean coherence is obtained in figure 5-(center), when dealing with a purely turbulent excitation. The interpretation of such result may be questionable. Indeed, in this case, as a turbulent component is only used as excitation field, it may be expected that the radiated field has to be well correlated with the excitation field. That underlines the misinterpretation of such tool analysis when dealing with uncorrelated source of noise. Such causality analysis performed thanks to the coherence function is only sensitive to punctual sound source which is not the case when the turbulent flow field contains a weakly spatial extent coherent sound source [3]. These observations confirm that the coherence function application could lead to misinterpretations.

We also observe that the mean coherence value computed between the radiated field and the acoustic field extracted from the aeroacoustic field (figure 5, bottom) is smaller that the one computed from calculations using a purely acoustic excitation (figure 5, top). That can be explained with the presence of the turbulent component when dealing with aeroacoustic excitation.

To investigate the coherence effect of the excitation on the vibroacoustic response of the plate, a spatially coherent excitation component is now superimposed to the aeroacoustic excitation. The excitation field is then composed of a diffuse component, a turbulent component and a plane wave component representing the coherent acoustic component. Diffuse field corresponds then to the other more *incoherent* acoustic sources. Moreover, two test cases are successively performed where the energy content of each excitation component is specified as follows:
test case 1: $S_{pp}^{Plane}(\omega) = S_{pp}^{Diffuse}(\omega) = 0.1 \times S_{pp}^{Corcos}(\omega)$

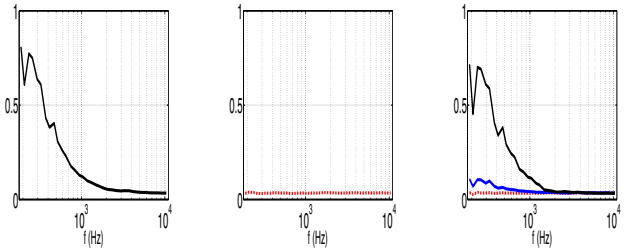

Figure 5: Mean coherence computed between the radiated pressure field and the diffuse acoustic component (left) or the turbulent component (center). Right: Mean coherence computed between the radiated pressure field and aeroacoustic excitation field. Black line: diffuse acoustic component. Red dotted line: turbulent component. Blue line: aeroacoustic (diffuse plus turbulent) component.

test case 2: $S_{pp}^{Plane}(\omega) = 0.1 \times S_{pp}^{Diffuse}(\omega) = 0.01 \times S_{pp}^{Corcos}(\omega)$. with $S_{pp}^{Plane}(\omega) = 0.6283 \text{Pa}^2.\text{rad}^{-1}.\text{Hz}^{-1}$ in each case.
For comparison, FEM computations are also performed with similar excitation fields but without plane wave coherent.

Figure 6 displays the PSD of the radiated pressure fluctuation at 0.6m from the plate and the transmission efficiency for the first test case. In these figures, the frequency x-axis is limited to 900Hz. It is observed that adding a plane wave component in the inlet excitation field leads to a great increase of the radiated noise, of a order of 7dB for high frequencies, even if the whole energy content of the inlet excitation field has increased of only 0.38dB. The transmission efficiency representation confirms this result. This is due to the presence of a plane wave component which is perfectly coherent having a very high level of transmission efficiency. It is then confirmed that the radiated field is quasi only due to the acoustic component of the excitation field (diffuse field and mainly plane wave field).
Similar conclusions can be done for the second test case even in presence of a very small increase (0.04dB due to plane wave) of the energy content of the whole excitation field [9].

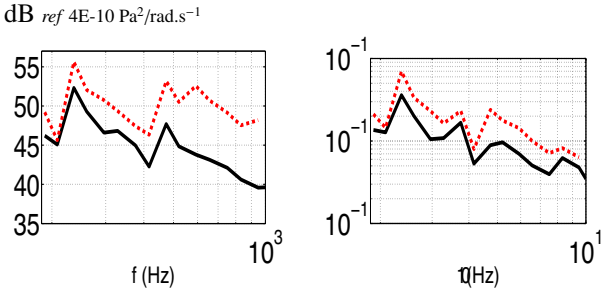

Figure 6: Right: PSD of the radiated acoustic pressure at 0.6m from the plate. Left: Transmission efficiency of the plate evaluated for different excitation fields. Black line: Diffuse field plus turbulent component satisfying $S_{pp}^{Diffus}(\omega) = 0.1 S_{pp}^{Corcos}(\omega)$. Dashed red line: Plane wave field plus Diffuse field plus turbulent component satisfying $S_{pp}^{Plane}(\omega) = S_{pp}^{Diffus}(\omega) = 0.1 S_{pp}^{Corcos}(\omega)$.

5 Conclusion

In this paper, we first propose the synthesis of the wall pressure field from the knowledge of the corresponding statistical properties (CPSD representation) of this field. Such synthesis based on a Cholesky decomposition and the imposition of random phase permits then to reproduce random spatial (acoustic and turbulent) pressure field impinging a plate. It is also demonstrated the potential of the synthesis procedure which can be also applied to inhomogeneous flow field which is generally observed on a car side window. About the inhomogeinity effect of the turbulent excitation on the vibroacoustic response, quasi-similar results are obtained when dealing with 'equivalent' homogeneous or inhomogeneous turbulent field.

Second, based on FEM calculations, the vibroacoustic behavior of a plate has been successively examined as a function of different types of excitation (acoustic, turbulent, aeroacoustic). Transmission efficiency analysis confirms that an acoustic excitation is more efficient than a turbulent excitation. Finally, present coherence function analysis emphasizes the limits of such analysis especially when dealing with uncorrelated sources of noise.

References

[1] B Arguillat, D. Ricot, C. Bailly, G. Robert, "Measured wavenumber-frequency spectrum associated with acoustic and aerodynamic wall pressure fluctuations", *J. Acoust. Soc. Am.* **128**(4), 1647-1655 (2010)

[2] W.K. Blake, *Mechanics of flow-induced sound and vibration, volumes I and II*, Acad. Press, London (1986)

[3] C. Bahr, L.N. Cattafesta, "Limits of coherence-based aeroacoustic analysis in the presence of distributed sources", *J. Acoust. Soc. Am* **129**(6), 248-253 (2011)

[4] P.G. Bremner, J.F. Wilby, "Aero-vibro-acoustics: problem statement and methods for simulation-based design solution", *8th AIAA/CEAS* paper 2551 (2002)

[5] G.M. Corcos, "Resolution of pressure in turbulence", *J. Acoust. Soc. Am* **35**, 192-199 (1963)

[6] J.P. Coyette, *Simulation of multi-correlated random processes using the FFT algorithm*, Free Field Technologies Technical report, Belgium (2002)

[7] A. Hekmati, *Analyse des événements aérodynamiques à l'origine des émissions sonores à partir de simulations numériques*, Thèse de l'Univ. Paris 6 (2011)

[8] A. Hekmati, D. Ricot, Ph. Druault, "Vibroacoustic behavior of a plate excited by synthetized aeroacoustic pressure fields", *16th AIAA/CEAS* paper 3950 (2010)

[9] A. Hekmati, D. Ricot, Ph. Druault, "Synthetized aeroacoustic wall pressure fields over a flat plate: generation, transmission and radiation analyses", *Submitted to J. Sound and Vib.* (2012)

[10] L.E. Wittig, K. Sinha, "Simulation of multicorrelated random processes using the FFT algorithm", *J. Acoust. Soc. Am* **58**(3), 630-634 (1973)

[11] *Actran 2004 Users guide*, Report. Free Field Technologies S.A., Belgium (2004)